Two-dimensional infrared spectroscopy of vibrational polaritons of molecules in an optical cavity

Prasoon Saurabh[a] and Shaul Mukamel[b]
Department of Chemistry, University of California, Irvine, California 92697, USA

(Received 28 December 2015; accepted 7 March 2016; published online 29 March 2016)

Strong coupling of molecular vibrations to an infrared cavity mode affects their nature by creating dressed polariton states. We show how the single and double vibrational polariton manifolds may be controlled by varying the cavity coupling strength and probed by a time domain two-dimensional infrared (2DIR) technique, double quantum coherence. Applications are made to the amide-I (CO) and amide-II (CN) bond vibrations of *N*-methylacetamide. © *2016 AIP Publishing LLC.* [http://dx.doi.org/10.1063/1.4944492]

I. INTRODUCTION

Elementary physical and chemical properties of molecules can be modified by coupling them to the optical modes of a cavity thus forming strongly coupled *matter* + *field* states known as polaritons.[1,2] These have been widely studied in atoms. Electronic polaritons in molecules have been extensively studied both experimentally and theoretically.[3–5] Vibrational polaritons in the infrared have been recently demonstrated in molecular aggregates[6–9] and in semiconductor nano-structures.[10–12] The radiation matter coupling is related to cavity frequency ω_c by $g_i = \sqrt{N}\boldsymbol{\mu}_i \cdot \boldsymbol{e}_c\sqrt{(\hbar\omega_c/2\epsilon_0 V)}$, where N is the number of molecules. $\boldsymbol{\mu}_i$ is the transition dipole moment of the mode i, $\boldsymbol{e}_c$ is the cavity electric field vector, ϵ_0 is the vacuum permittivity, and V is the cavity mode volume.[1,6–9,13,14] While strong coupling to cavity modes has been realized even for a single atom, $N = 1$,[1,2,15] polaritons in organic molecules were reported for large $N(\sim 10^{17})$.[6] With the advent of anomalous refractive index materials,[16,17] sub-wavelength Fabry-Perot microcavities,[18] and nanocavities,[19] it may become possible to achieve strong cavity coupling of single molecules.

Coherent multidimensional infrared spectroscopy is a powerful time domain tool that can probe anharmonicities and vibrational energy relaxation pathways.[20–24] Vibrational polaritons were experimentally reported[6,8,9] and calculated[7,25] recently. Multidimensional spectroscopic studies for electronically excited states in semiconductor cavity for nano-particles like $In_{0.04}Ga_{0.96}As$ have been demonstrated.[12,27] Similarly, electronic exciton-polariton interactions of quantum wells in microcavity[28] have also been reported. Bipolaritons generated using four wave mixing techniques have been used as efficient entangled photon source.[29,30]

In this article, we calculate 2DIR signals for vibrational polaritons, focusing especially on the double quantum coherence (DQC) technique. Studying DQC of molecular vibrational polaritons in optical cavity can be used to study the effects of strong couplings on the vibrational anharmonicities and consequently allow us to control these anharmonicities. We introduce DQC signal in Sec. II, we then study single vibrational mode (amide-I of *N*-methylacetamide (NMA)) coupled to a single mode cavity and calculate DQC in Sec. III, followed by two vibrational modes (amide-I+II of NMA) coupled to a single mode cavity (Sec. IV), and finally conclude in Sec. V.

II. VIBRATIONAL POLARITONS AND THEIR DQC SIGNAL

Vibrational modes (Fig. 1) coupled to an infrared cavity under the Rotating Wave Approximation (RWA) are described by the Hamiltonian,[6–9,31–33]

$$H_0 = \omega_c(\theta)a^\dagger a + \sum_i^m \omega_i b_i^\dagger b_i + \sum_{i\neq j}^m J_{ij} b_i^\dagger b_j - \sum_{ij}^m \frac{\Delta_{ij}}{2} b_i^\dagger b_j^\dagger b_i b_j + \sum_{i=1}^m g_i \left(a^\dagger b_i + b_i^\dagger a\right), \quad (1)$$

where $a(a^\dagger)$ and $b(b^\dagger)$ are annihilation (creation) operators for the cavity photon and vibrational excitation, respectively, which satisfy boson commutation relations, $[a, a^\dagger] = 1; [b_i, b_j^\dagger] = \delta_{ij}$ and $\hbar = 1$. $\omega_c(\theta) = \omega_0\left(1 - \frac{\sin^2(\theta)}{n_{eff}^2}\right)^{-1/2}$ is the angle-dependent cavity energy with ω_0 being cavity cutoff (or maximum) energy and θ the angle of incidence to the cavity mirrors. We set $\theta = 0°$ for simplicity. ω_i is vibrational frequency of mode i. J_{ij} is the scalar coupling between two vibrational modes i and j, while Δ_{ij} is the anharmonicity between respective modes. Finally, the coupling strength of vibrational modes i to an optical mode is g_i as described in the Introduction.

The cavity volume ($V = (\lambda/n_{eff})^3$) depends on cavity resonance wavelength (λ) and effective intra-cavity refractive index (n_{eff}).[1,13,14] Decreasing n_{eff} can also be used for strong coupling to single molecular vibrational excitation, for instance, when the refractive indices of one of the two layers' of a Distributed Bragg Reflector (DBR) Fabry-Perot are equal to the empty cavity refractive index n_c, say $n_c = (n_2 \veebar n_1)$, then $n_{eff} = \sqrt{n_1 n_2}$. In this case, choosing either one of the layers

[a]Electronic mail: psaurabh@uci.edu
[b]Electronic mail: smukamel@uci.edu

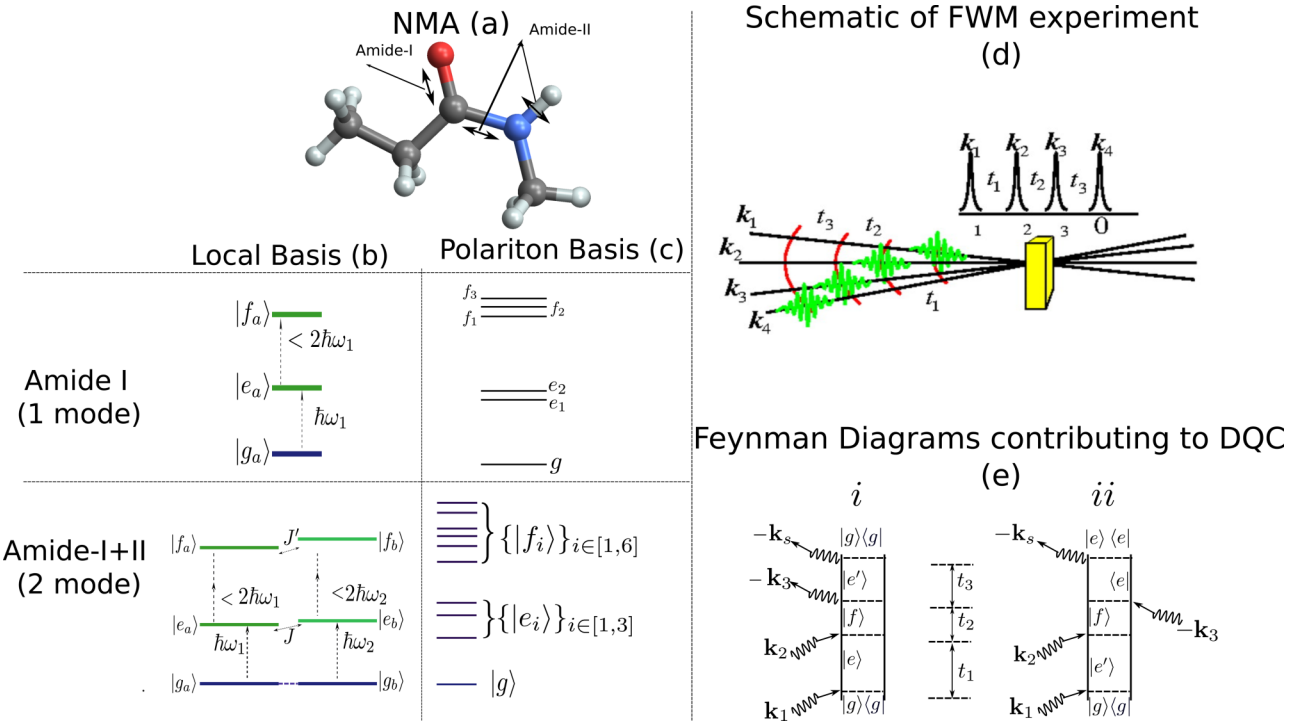

FIG. 1. Amide-I (C=O symmetric stretch) and amide-II (CN symmetric stretch + NH bend) vibrations are represented using double sided arrow for N-methylacetamide in (a). Eigen-energies of amide-I and coupled amide-I and amide-II motifs in local basis and polariton basis (see Sec. SI of the supplementary material[34] for detail) are given in (b) and (c), respectively. (d) schemes the FWM experiment, the yellow sample is the DBR Fabry-Perot cavity coupled to molecular vibrations (see text for detail) and (e) shows the relevant ladder diagrams contributing to double quantum coherence (DQC) technique.

to be material with anomalous refractive index may decrease $n_{eff} < 1$.[18] The vacuum Rabi splitting Ω_R of mode i is $2\hbar g_i$.

DQC is a four wave mixing signal generated by three chronologically ordered pulses with wavevectors $\boldsymbol{k}_1$, $\boldsymbol{k}_2$, and $\boldsymbol{k}_3$ and detected by with a fourth pulse in the direction, $\boldsymbol{k}_{III} = \boldsymbol{k}_1 + \boldsymbol{k}_2 - \boldsymbol{k}_3$ (Fig. 1(e)).[21,26] The signal is recorded versus three time delays t_1, t_2, and t_3. We assume a three polariton manifold as shown in Fig. 1. Using the ladder diagrams for DQC (Fig. 1(e)) in polariton basis, which diagonalizes the first three and last terms of Eq. (1) (Fig. 1, Sec. SI of the supplementary material[34]), we see that system oscillates with frequency $\Omega_{eg} = \Omega_e - \Omega_g$ during time delay $t_1 = \tau_2 - \tau_1$ and with frequency $\Omega_{fe} = \Omega_f - \Omega_e$ during delay $t_2 = \tau_3 - \tau_2$ in both contributing diagrams (Fig. 1(e)). After the third pulse, the system oscillates either with frequency $\Omega_{e'g}$ or $\Omega_{e'f}$ during the delay $t_3 = \tau_4 - \tau_3$. For harmonic case, $\Omega_{e'g} = \Omega_{e'f}$ where the DQC signal vanishes. A 3D signal $\mathcal{S}(t_3,t_2,t_1)$ which can be written as double Fourier transform with respect to t_2 and t_3 as[21]

$$\mathcal{S}(\Omega_3,\Omega_2,t_1) = \int\int_0^\infty dt_3 dt_2 e^{i(\Omega_3 t_3 + \Omega_2 t_2)} \mathcal{S}(t_3,t_2,t_1). \quad (2)$$

Upon expanding in polariton eigenstates, the signal with time delay $t_1 = 0$ becomes

$$\mathcal{S}(\Omega_3,\Omega_2,t_1=0) = \sum_{ee',f} \frac{1}{(\Omega_2 - \Omega_{fg} + i\gamma_{fg})} \times \left[\mu_{e'f}\mu_{ge'}\mu_{fg}\mu_{ge} \frac{1}{\Omega_3 - \Omega_{e'g} + i\gamma_{e'g}} - \mu_{ge'}\mu_{e'f}\mu_{fg}\mu_{eg} \frac{1}{\Omega_3 - \Omega_{fe} + i\gamma_{fe}} \right], \quad (3)$$

where μ_{ij} is the polariton transition dipole from states in manifold $j \to i$ while γ_{ij} is the respective dephasing. Note that the polariton eigenstates depend on the effective cavity coupling strengths, $\widetilde{g}_i \left(=\sqrt{N g_i^2 - \frac{1}{4}(\kappa - \gamma_i)^2}\right)$, where κ is cavity decay rate, and γ_i is dephasing rate of respective mode.[13] Tuning the cavity coupling allows to control spectral structures of the singly and doubly excited vibrational polariton manifolds (Fig. 2) and can be captured using DQC as illustrated in Sec. III.

III. A SINGLE VIBRATIONAL MODE COUPLED TO SINGLE CAVITY MODE

The amide motifs (O=C—N—H) link the amino-acid in peptides containing fundamental structural information, for instance, backbone geometry, interactions with hydrogen bonds, and dipole-dipole interactions.[35] 2D spectroscopy of the amide-I and II symmetric vibrations (Fig. 1(e)) has been studied.[20,36] We focus on the amide-I vibrations in NMA (Table I). We consider a single amide-I stretch mode in resonance with the cavity mode and large anharmonicity ($\Delta_{ij} > \gamma_{ij}$) with varying coupling strengths $\widetilde{g}_1$ ranging from 0 to 80 cm^{-1} (Table I). For a single vibrational mode (Fig. 1), the three polariton manifolds have a ground state (g), two single excited states (e), and three doubly excited states (f). Furthermore, for detuning ($\delta = \omega_1 - \omega_c$), the polariton basis modifies the anharmonicity $\Delta_{11} (\to \widetilde{V}_{11} = 16\Delta_{11}|\widetilde{g}_1^4/(\delta^2 - 16\widetilde{g}_1^2)^2|)$.

Using Eq. (3) and ladder diagrams (Fig. 1(e)), the signals $|\mathcal{S}_i(\Omega_3,\Omega_2,0)|$, $|\mathcal{S}_{ii}(\Omega_3,\Omega_2,0)|$, and $|\mathcal{S}(\Omega_3,\Omega_2,0)$

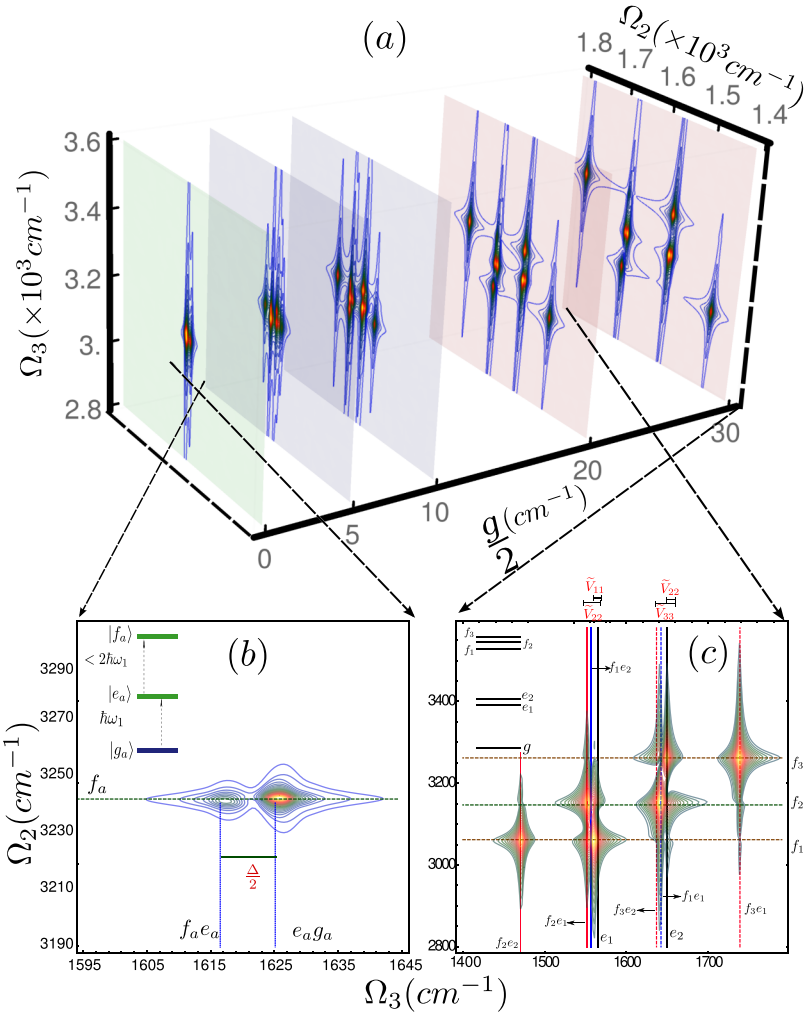

FIG. 2. (a) Absolute value of DQC signal (Eq. (3)) for amide-I vibrations of NMA, as we vary coupling strength (g) from no (green plane), weak (blue planes), and strong (red planes) coupling regimes. (b) Schematic representation of DQC signal (zoomed in the grey square at $g = 0$ cm^{-1}) with all possible peaks identified as intersections of different lines. (c) Same result but for strong coupling and the last panel. The lines are as follows: (i) Ω_{fe} labelled as $f_i e_j$ (dashed blue lines), (ii) Ω_{eg} labelled as e_j (black solid lines), (iii) Ω_{fg} labelled as f_i and appropriate anharmonicities (Δ_{ij} in local basis or $\widetilde{V}_{ii}$ in polariton basis), respectively. We wish to spectrally resolve (b) to (c).

$= |\mathcal{S}_i(\Omega_3,\Omega_2,0) + \mathcal{S}_{ii}(\Omega_3,\Omega_2,0)|$ are shown in Figs. 3 and 4 in left, center, and right columns, respectively (Sec. III). Absolute values are shown to illustrate peak assignments and effects of varying coupling strengths ($\widetilde{g}_i$). For completeness, the respective absorptive (Im) and dispersive (Re) parts of the DQC signals are shown in Sec. SIIIA in Ref. 34. The peak splittings depend on coupling strengths ($\widetilde{g}_i$) and polariton anharmonicities ($\widetilde{V}_{ij}$) and are given in Sec. SV of Ref. 34.

TABLE I. Parameters used in this work. ω_0 is cavity cut-off frequency. $\omega_{1,2}$ are vibrational exciton (1,2) (amide-I, amide-II) energies,[37,38] $\gamma_{1,2}$ are their respective dephasing rates, J_{ij} is harmonic scalar coupling, and Δ_{ij} are exciton-exciton interaction energies.

(in cm^{-1})	Cavity	Amide-I	Amide-I+II
Energy	$\omega_0 = 1625$	$\omega_1 = 1625$	$\omega_1 = 1625, \omega_2 = 1545$
Dephasing	$\kappa = 0$	$\gamma_1 = 20$	$\gamma_1 = \gamma_2 = 20$
Anharmonicities (local basis)	$\Delta_{00} = 0$	$\Delta_{11} = 15$	$\Delta_{11} = 15, \Delta_{22} = 11$ $\Delta_{21} = \Delta_{12} = 10$
Scalar coupling	...	...	$J_{12} = 15$
Effective refractive index	$n_{eff} = 0.5$	...	...
Anharmonicities (polariton basis)	$\widetilde{V}_{ij} = \frac{\Delta_{ij}}{2}\lvert X_i\rvert^2\lvert X_j\rvert^2$		

Free molecule (Fig. 3): The amide-I vibrations in NMA (without cavity) are a simple three level system as shown in Fig. 1. Under this condition, $e_1 = e_2$ and $f_1 = f_2 = f_3$, thus we only observe single peak resonant at $\Omega_{fg} = 3168$ cm^{-1} on Ω_2 axis. The peaks due to $|\mathcal{S}_i(\Omega_3,\Omega_2,0)|$ (Fig. 3(a)) show $\Omega_{eg} = 1625$ cm^{-1} resonance, while $|\mathcal{S}_{ii}(\Omega_3,\Omega_2,0)|$ (Fig. 3(b)) shows resonance at $\Omega_{fe} = 1617$ cm^{-1} along Ω_3 axis. The total signal (Fig. 3(c)) thus shows two peaks due to resonances at Ω_{eg} and Ω_{fe}.

Weak coupling regime (Fig. 4(top row)) *with* $\widetilde{g} = 20$ cm^{-1}: Upon varying the coupling strength, there are two singly excited and three doubly excited polariton states (Figs. 1(b) and 1(c), Sec. SII-S1 of Ref. 34). We thus observe that all $|\mathcal{S}_i(\Omega_3,\Omega_2,0)|$, $|\mathcal{S}_{ii}(\Omega_3,\Omega_2,0)|$, and $|\mathcal{S}(\Omega_3,\Omega_2,0)|$ show three distinct peaks along Ω_2 axis with energies resonant to $\Omega_{f_1g} = 2\Omega_{e_1g} - \widetilde{V}_{11}$, $\Omega_{f_2g} = 2\Omega_{e_1g}$, and $\Omega_{f_3g} = 2\Omega_{e_2g} - \widetilde{V}_{33}$, respectively. Along Ω_3 axis, $|\mathcal{S}_i(\Omega_3,\Omega_2,0)|$ (Fig. 4(top, left)) shows peak resonance at Ω_{e_1g} and Ω_{e_2g} with splitting $\sim\widetilde{g}$. The $|\mathcal{S}_{ii}(\Omega_3,\Omega_2,0)|$ (Fig. 4(top, middle)) has six distinct peaks at energies resonant to Ω_{f_2,e_2}, Ω_{f_2,e_1}, Ω_{f_1,e_2}, Ω_{f_3,e_2}, Ω_{f_1,e_1}, Ω_{f_3,e_1} in increasing order, respectively. The $|\mathcal{S}(\Omega_3,\Omega_2,0)|$ (Fig. 4(top, right)) has diminished peaks at $\Omega_{f_2e_1}$ and $\Omega_{f_3e_2}$

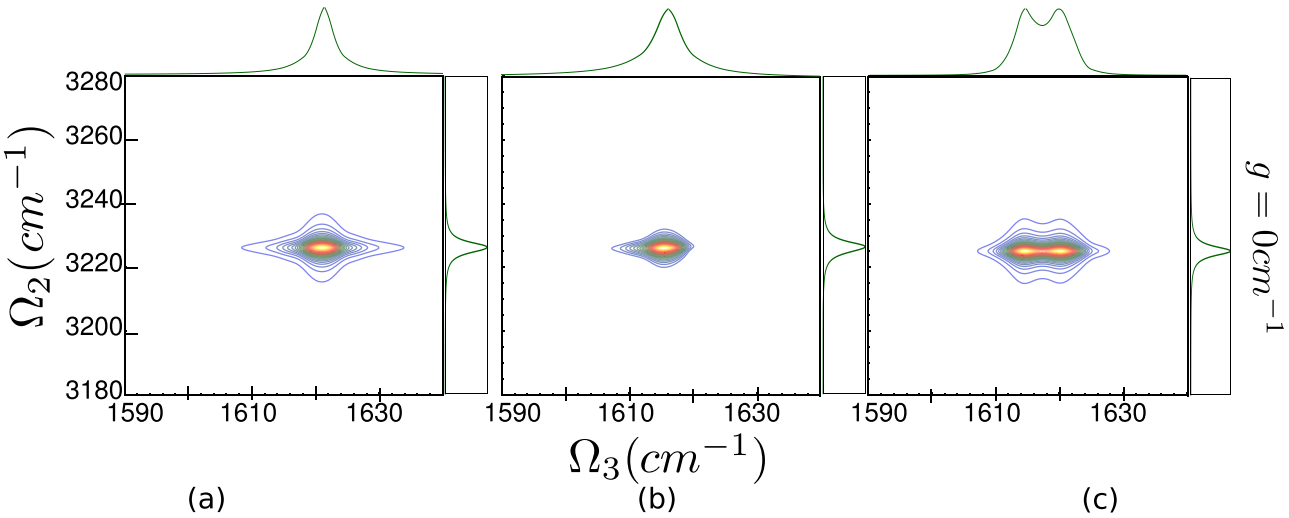

FIG. 3. DQC signals for amide-I vibrations in NMA using Eq. (3) and ladder diagrams (Fig. 1(e)). (a) $|\mathcal{S}_i(\Omega_3,\Omega_2,0)|$ with resonance at $\Omega_{eg} = 1625$ cm^{-1}, (b) $|\mathcal{S}_{ii}(\Omega_3,\Omega_2,0)|$ with resonance at $\Omega_{fe} = 1617$ cm^{-1}, and (c) $|\mathcal{S}(\Omega_3,\Omega_2,0)|$ with resonances at $\Omega_{eg} = 1625$ cm^{-1} and $\Omega_{fe} = 1617$ cm^{-1}. The linear projections along each axis are shown in green. For simplicity, cavity field vector $\boldsymbol{e}_c$ is assumed to be mostly parallel to molecular vibrational transition dipole $\boldsymbol{\mu}_m$. Amide-I vibrations (ω_1) are resonant to cavity cutoff frequency $\omega_0 = 1625$ cm^{-1}. The anharmonicity is assumed $\Delta_{11} = 15$ cm^{-1} (Table I).

due to destructive interference of $\Omega_{f_2e_1}$ with Ω_{e_1g} and $\Omega_{f_3e_2}$ with Ω_{e_2g} resonances.

Strong coupling regime (Fig. 4(bottom row)) *with* $\widetilde{g} = 50$ cm^{-1}: The signals corresponding to $|\mathcal{S}_i(\Omega_3,\Omega_2,0)|$ (Fig. 4(bottom, left)), $|\mathcal{S}_{ii}(\Omega_3,\Omega_2,0)|$ (Fig. 4(bottom, middle)), and $|\mathcal{S}(\Omega_3,\Omega_2,0)|$ (Fig. 4(bottom, right)) show peaks corresponding to Ω_{f_1g}, Ω_{f_2g}, and Ω_{f_3g} along Ω_2 axis. Projections on Ω_3 axis for $|\mathcal{S}_{ii}(\Omega_3,\Omega_2,0)|$ six peaks assigned as in weak coupling case, however the peak splitting between resonance pairs with energies $(\Omega_{f_2e_1},\Omega_{f_1e_2})$ and $(\Omega_{f_3e_2},\Omega_{f_1e_1})$

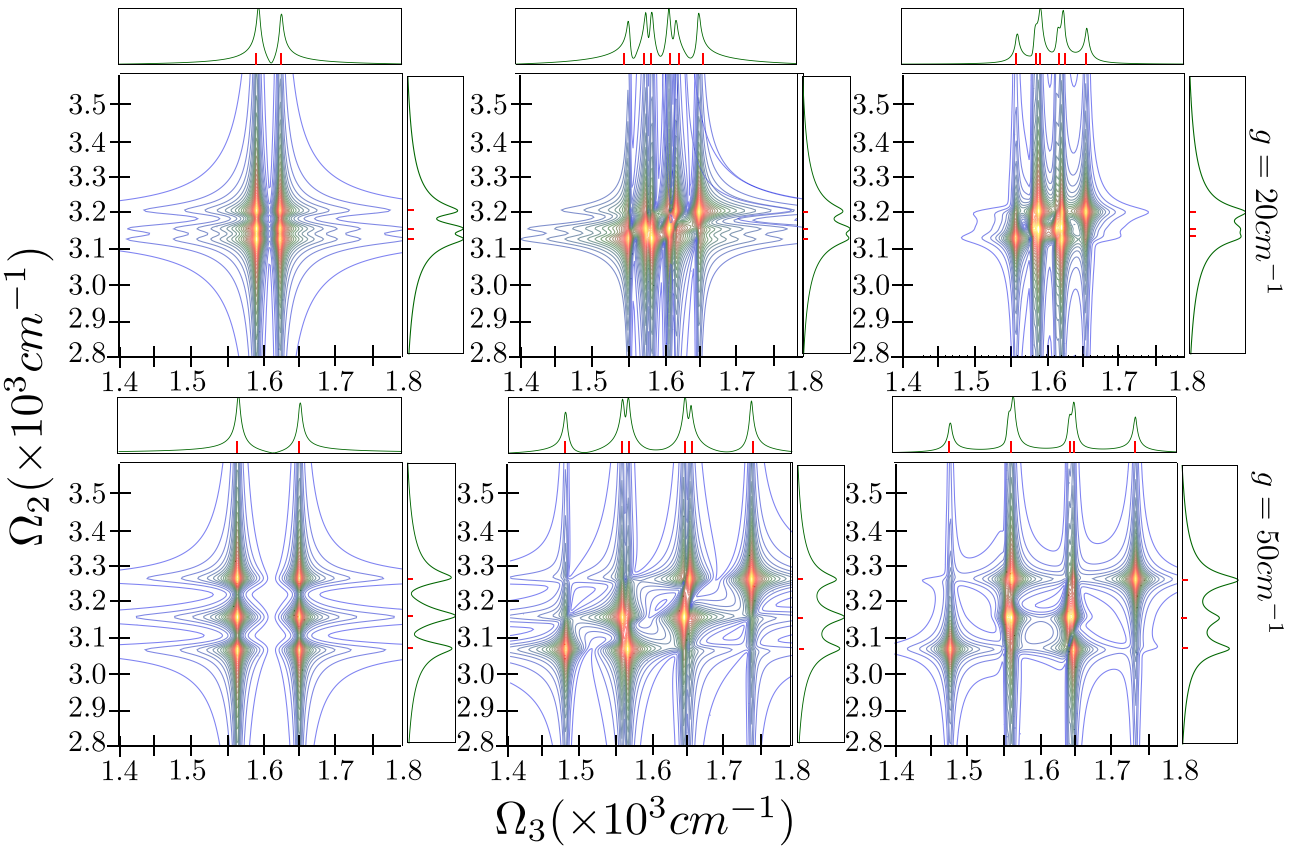

FIG. 4. DQC signals using Eq. (3) and ladder diagrams (Fig. 2(b)). Columns (left-) $|\mathcal{S}_i(\Omega_3,\Omega_2,0)|$ with resonance at Ω_{e_1g} and Ω_{e_2g}; (middle-) $|\mathcal{S}_{ii}(\Omega_3,\Omega_2,0)|$ with resonance at Ω_{f_2,e_2}, Ω_{f_2,e_1}, Ω_{f_1,e_2}, Ω_{f_3,e_2}, Ω_{f_1,e_1}, Ω_{f_3,e_1}; and (right-) $|\mathcal{S}(\Omega_3,\Omega_2,0)|$ with respective resonances for amide-I vibrations in NMA with cavity coupling rows: (a) 20 cm^{-1} and (a) 50 cm^{-1}. The linear projections along each axis are shown in green. For simplicity, cavity field vector $\boldsymbol{e}_c$ is assumed to be mostly parallel to molecular vibrational transition dipole $\boldsymbol{\mu}_m$. Amide-I vibrations (ω_1) are resonant to cavity cutoff frequency $\omega_0 = 1625$ cm^{-1}. The anharmonicity is assumed $\Delta_{11} = 15$ cm^{-1} (Table I).

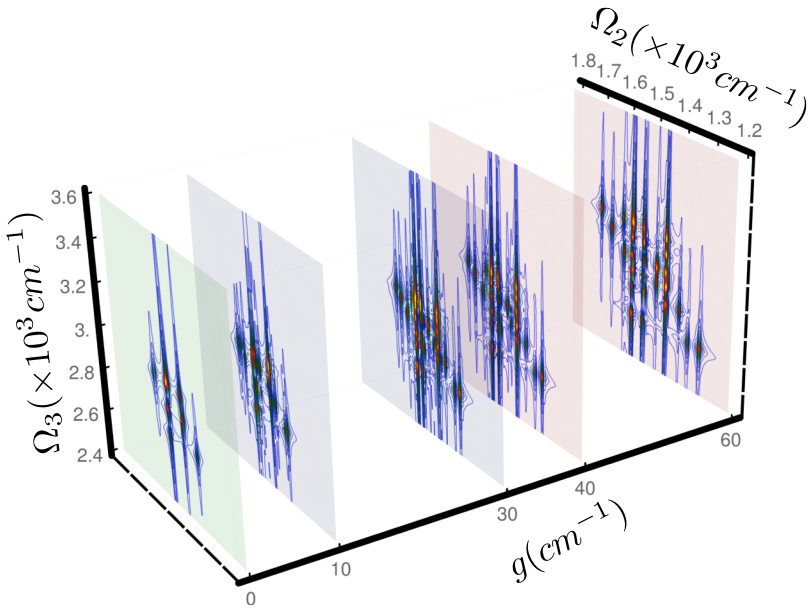

FIG. 5. Modulus of DQC signal for amide-I+II vibrations in NMA with varying cavity coupling (0 cm^{-1} $\rightarrow$ 60 cm^{-1}). Cavity field vector $\boldsymbol{e}_c$ is assumed to be mostly parallel to molecular vibrational transition dipole μ_m. Amide-I vibrations (ω_1) are resonant to cavity cutoff frequency $\omega_0 = 1625$ cm^{-1} and $\omega_2 = 1540$ cm^{-1}. The anharmonicities $\Delta_{11} = 15$ cm^{-1} and $\Delta_{22} = 11$ cm^{-1} (Table I).

remains relatively constant and proportional to respective contributing anharmonicities. The total signal shows six peaks due to $\Omega_{f_2e_1}$ and $\Omega_{f_3e_2}$ diminished because of destructive interferences from resonances of singly excited polaritons.

This partial cancellation of peaks puts an upper bound on strong coupling strengths for fully resolved DQC signals. Furthermore by changing t_1, we can observe the dynamics in singly and doubly excited polariton manifolds to obtain bountiful information regarding lifetimes of molecular vibrational bipolaritons. In case of zero detuning ($\delta = \omega_1 - \omega_c = 0$), the doublet peak splitting due to $\widetilde{V}_{11}$ is independent of coupling strength, i.e.,$\widetilde{V}_{11} = \Delta/32$. Thus DQC can be used as direct measurements of anharmonicities due to vibrational polariton-polariton interactions for vanishing detuning cases. One has to be careful, however, for $\delta \neq 0$ cases, as such conditions allow the anharmonicities to vary non-trivially ($\sim 16\Delta_{11}|\widetilde{g}_1^4/(\delta^2 - 16\widetilde{g}_1^2)^2|$). This may cause destructive interference of different peaks along Ω_3 axis.

IV. POLARITONS FOR TWO VIBRATIONAL MODES AND THEIR DQC SIGNAL

We now couple the amide-I and amide-II vibrations (Fig. 1, Ref. 36) of a single NMA molecule ($N = 1$) to an infrared cavity. We next calculate the DQC signals for vibrational molecular polaritons (Fig. 1(e), Eq. (3)) utilizing Eqs. (S2)-(S5) of the supplementary material.[34]

The overlapping of peaks due to anharmonicities is better illustrated in case of amide-I+II vibrations coupled to single mode cavity. We next present three coupling regimes for such a condition. We assume $\widetilde{g}_1/\widetilde{g}_2 = constant$ for simplicity. The remainder of relevant parameters is shown in Table I.

No cavity (Fig. 6(a)): The coupled amide-I+II vibrations of NMA are effectively a three level system with two singly excited states and three doubly excited states in absence of cavity coupling. The two singly excited states are resonant with Ω_{e_1g} and $\Omega e_2 g$. The three doubly excited states are resonant with frequencies $\Omega_{f_1g} = 2\Omega_{e_1g} - \Delta_{11}$, $\Omega_{f_2g} = \Omega_{e_1g} + \Omega_{e_2g}$, and $\Omega_{f_3g} = 2\Omega_{e_2g} - \Delta_{22}$ (Sec. SII of the supplementary material,[34] Table I). These peaks are observed along Ω_2 axis. Whereas we only observe four peaks along Ω_3 axis in Fig. 6((a), right column) because the tuples $((\Omega_{f_2e_1}, \Omega_{f_1e_2}), \Omega_{e_1g})$ and $((\Omega_{f_3e_2}, \Omega_{f_1e_1}), \Omega_{e_2g})$ cannot be resolved due to anharmonicities (Δ_{ii}, Table I).

Weak coupling regime with $\widetilde{g} = 10$ cm^{-1} (Fig. 6(b)): Under these conditions, we observe five peaks along Ω_2 axis corresponding to Ω_{f_1g},Ω_{f_2g},Ω_{f_3g},Ω_{f_4g},$\Omega_{f_5g} = \Omega_{f_6g}$. Projections along Ω_3 axis show two peaks for $|\mathcal{S}_i(\Omega_3, \Omega_2, 0)|$ (Fig. 6((b), left column)) resonant with frequencies Ω_{e_1g}, $\Omega_{e_2g} \approx \Omega_{e_3g}$. For $|\mathcal{S}_{ii}(\Omega_3, \Omega_2, 0)|$ (Fig. 6((b), middle column)), we would ideally expect eighteen peaks corresponding to $\Omega_{f_1e_3}$, $\Omega_{f_1e_2}$, $\Omega_{f_3e_4}$, $\Omega_{f_4e_2}$, $\Omega_{f_2e_3}$, $\Omega_{f_2e_2}$, $\Omega_{f_1e_1}$, $\Omega_{f_3e_3}$, $\Omega_{f_3e_2} = \Omega_{f_4e_1} = \Omega_{f_6e_3}$, $\Omega_{f_6e_2}$, $\Omega_{f_5e_3}$, $\Omega_{f_2e_1}$, $\Omega_{f_5e_2}$, $\Omega_{f_3e_1}$, $\Omega_{f_6e_1}$, $\Omega_{f_5e_1}$ in energetically increasing order. However, only twelve peaks are observed due to overlapping caused by anharmonicities and coupling strength. Similar to amide-I vibrations of NMA in cavity, we observe fewer peaks in $|\mathcal{S}(\Omega_3, \Omega_2, 0)|$ (Fig. 6((b), right column)) than that of $|\mathcal{S}_{ii}(\Omega_3, \Omega_2, 0)|$ due to destructive interferences between $|\mathcal{S}_{ii}(\Omega_3, \Omega_2, 0)|$ and $|\mathcal{S}_i(\Omega_3, \Omega_2, 0)|$.

Strong coupling regime $\widetilde{g} = 50$ cm^{-1} (Fig. 6(c)): Increasing coupling resolves the six bipolariton resonances along Ω_2 for all contributions to the DQC signal (Fig. 6(c)). Along Ω_3 axis, however, only $|\mathcal{S}_i(\Omega_3, \Omega_2, 0)|$ is more resolved with three peaks corresponding to Ω_{e_1g}, Ω_{e_2g}, and Ω_{e_3g} with splitting $\sim\widetilde{g}_i$. Despite better peak resolution due to coupling strength dependent peak separations, resonances due to overlapping peaks cannot be fully resolved. The total signal (Fig. 6(right column)) only has 10 distinct peaks as a result of destructive interference of energies of Ω_{e_2g} and Ω_{e_3g} with some of the resonances from $|\mathcal{S}_{ii}(\Omega_3, \Omega_2, 0)|$.

Increasing coupling strengths provides us well resolved molecular vibrational bipolariton manifold structure (along Ω_2 axis); however, it may not provide well resolved DQC signals along Ω_3 axis requiring a careful tuning of $\widetilde{g}_i$.

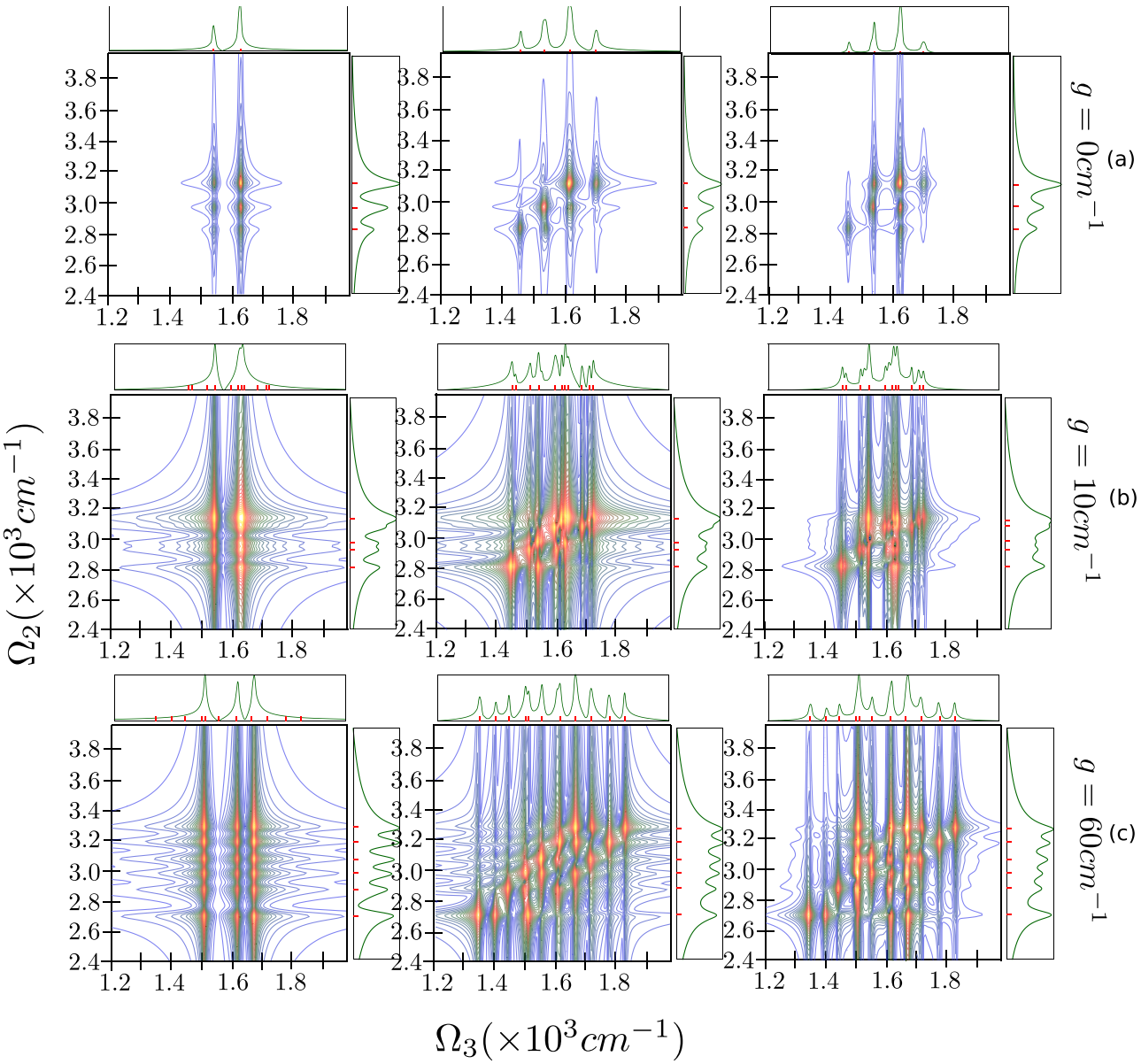

FIG. 6. DQC signals for amide-I+II vibrations in NMA using Eq. (3) and ladder diagrams (Fig. 1(e)): Columns: (left-) $|S_i(\Omega_3,\Omega_2,0)|$ with resonance at Ω_{e_1g}, Ω_{e_2g}, and Ω_{e_3g}; (middle-) $|S_{ii}(\Omega_3,\Omega_2,0)|$ with resonance at $\Omega_{f_1e_3}\approx\Omega_{f_1e_2}$, $\Omega_{f_3e_4}\approx\Omega_{f_4e_2}$, $\Omega_{f_2e_3}\approx\Omega_{f_2e_2}$, $\Omega_{f_1e_1}$, $\Omega_{f_3e_3}\approx\Omega_{f_3e_2}=\Omega_{f_4e_1}=\Omega_{f_6e_3}$, $\Omega_{f_6e_2}$, $\Omega_{f_5e_3}$, $\Omega_{f_2e_1}$, $\Omega_{f_5e_2}$, $\Omega_{f_3e_1}$, $\Omega_{f_6e_1}$, $\Omega_{f_5e_1}$ and (right-) $|\mathcal{S}(\Omega_3,\Omega_2,0)|$ with respective resonances and cavity couplings (rows) (a) 0 cm^{-1}, (b) 10 cm^{-1}, and (c) 60 cm^{-1} along Ω_3, while peaks at Ω_{f_1g},Ω_{f_2g},Ω_{f_3g},Ω_{f_4g},Ω_{f_5g}, and Ω_{f_6g} along Ω_2. The linear projections along each axis are shown in green. For simplicity, cavity field vector $\boldsymbol{e}_c$ is assumed to be mostly parallel to molecular vibrational transition dipole $\boldsymbol{\mu}_m$. Amide-I vibrations (ω_1) are resonant to cavity cutoff frequency $\omega_0 = 1625$ cm^{-1} and $\omega_2 = 1540$ cm^{-1}. The anharmonicities are assumed $\Delta_{11} = 15$ cm^{-1} and $\Delta_{22} = 11$ cm^{-1} (Table I).

V. CONCLUSIONS

The multidimensional DQC signals shown in Figs. 2-6 demonstrate how the ground state vibrational excitation manifolds are modified upon coupling to the cavity modes. The anharmonicities in the case of amide-I of NMA coupled to cavity (for non-zero detuning $\delta \neq 0$) are modified with cavity coupling strength, $\Delta_{ij} \to \widetilde{V}_{ij} = 16\Delta_{11}|\widetilde{g}_1^4/(\delta^2 - 16\widetilde{g}_1^2)^2|$ and this can be observed in the peak splitting. For zero detuning, the anharmonicity is independent of coupling strength, i.e., $\lim_{\delta\to 0}\widetilde{V}_{ij} = \Delta_{11}/32$. However, in the case of amide-I+II of NMA coupled to the infrared cavity anharmonicities in polariton basis varying nontrivially by $\widetilde{V}_{ij} = 1/2\Delta_{ij}|X_i|^2|X_j|^2$, where $X_{i/j}$ depend on higher order of coupling strengths. This causes several peaks to overlap beyond certain cavity coupling and this is why not all expected peaks for Ω_{fe} can be spectrally resolved in Fig. 6. However, we can use cavity coupling dependent anharmonicities for modifications of ground vibrational structures to mimic weakly interacting molecular vibrational multi-modes.

Controlling and manipulating lifetime of single molecular vibrations by tuning the coupling strengths and time delays between ultrafast pulses (say, t_1) can reveal new energy transfer mechanisms. Varying cavity polarization ($\boldsymbol{\mu}_k \cdot \boldsymbol{e}_c$) and incident angle ($\theta$) in Eq. (1) using collinear experiments[27] could provide information regarding spatial confinements of several vibrational excitations and possibilities of molecular vibrational condensates like usual electronic polariton

condensates in organic[39–41] and inorganic[39,42,43] microcavities, if effective dense vibrational polaritons are obtained, which may be possible in larger macromolecules like J-aggregates. Time-varying cavity coupling strengths can be used to study dynamics of efficient cooling of molecular vibrational states for $n-$ *polariton* manifolds using higher dimensional spectroscopic techniques.

This work can be extended to control collective molecular vibrational excitations, which may be a useful tool in molecular cooling[44] allowing to perform ultracold experiments even at room-temperature. Furthermore, by varying the time delays, one could be able to modify molecular vibrations via cavity and catch them in action in real time. We show that, by varying the cavity coupling strength ($\tilde{g}$), it is possible to retrieve spectrally well-resolved molecular vibrational polariton (bipolariton) resonances which are otherwise difficult to resolve (see Figs. 2-6, for example). Similar results with respect of the anharmonicities and peak redistributions due to cavity coupling can be achieved using other 2DIR techniques, e.g., $\boldsymbol{k}_s = -\boldsymbol{k}_1 + \boldsymbol{k}_2 + \boldsymbol{k}_3$ or $\boldsymbol{k}_s = \boldsymbol{k}_1 - \boldsymbol{k}_2 + \boldsymbol{k}_3$; however, the full power of DQC measurements presented here for single molecule in optical cavity can be seen more easily for macromolecules. For such larger systems, a different and much faster numerical algorithms utilizing techniques similar to Nonlinear Exciton Equations (NEEs)[32] will be useful. Studying the dynamics of modified electronic ground states by applying methods developed in Ref. 26 can also be done. In addition, incorporating electronic states can similarly be achieved to modify vibrational excitations of electronically excited states.

ACKNOWLEDGMENTS

We wish to thank Dr. Markus Kowalewski for valuable comments. The authors gratefully acknowledge the support of National Science Foundation (Grant No. CHE-1361516) and the Chemical Sciences, Geosciences, and Biosciences Division, Office of Basic Energy Sciences, Office of Science, U.S. Department of Energy through Award No. DE-FG02-4ER15571. The computational resources were provided by DOE.

[1]P. R. Berman, *Cavity Quantum Electrodynamics* (Academic Press, Inc., Boston, MA, 1994).
[2]S. Haroche and J. M. Raimond, *Exploring the Quantum* (Oxford University Press, 2006).
[3]D. M. Coles, Y. Yang, Y. Wang, R. T. Grant, R. A. Taylor, S. K. Saikin, A. Aspuru-Guzik, D. G. Lidzey, J. K.-H. Tang, and J. M. Smith, Nat. Commun. **5**, 5561 (2014).
[4]D. M. Coles, N. Somaschi, P. Michetti, C. Clark, P. G. Lagoudakis, P. G. Savvidis, and D. G. Lidzey, Nat. Mater. **13**, 712 (2014).
[5]F. Herrera, B. Peropadre, L. A. Pachon, S. K. Saikin, and A. Aspuru-Guzik, J. Phys. Chem. Lett. **5**, 3708 (2014).
[6]A. Shalabney, J. George, J. Hutchison, G. Pupillo, C. Genet, and T. W. Ebbesen, Nat. Commun. **6**, 5981 (2015).
[7]J. del Pino, J. Feist, and F. J. Garcia-Vidal, New J. Phys. **17**, 053040 (2015).
[8]A. Shalabney, J. George, H. Hiura, J. A. Hutchison, C. Genet, P. Hellwig, and T. W. Ebbesen, Angew. Chem., Int. Ed. **54**, 7971 (2015).
[9]B. Simpkins, K. P. Fears, W. J. Dressick, B. T. Spann, A. D. Dunkelberger, and J. C. Owrutsky, ACS Photonics **2**, 1460 (2015).
[10]T. Autry, G. Nardin, D. Bajoni, A. Lemaître, S. Bouchoule, J. Bloch, and S. Cundiff, *CLEO: QELS_Fundamental Science* (Optical Society of America, 2015), p. FW4B–7.
[11]Y. Sun, Y. Yoon, M. Steger, G. Liu, L. N. Pfeiffer, K. West, D. W. Snoke, and K. A. Nelson, preprint arXiv:1508.06698 (2015).
[12]B. L. Wilmer, F. Passmann, M. Gehl, G. Khitrova, and A. D. Bristow, Phys. Rev. B **91**, 201304 (2015).
[13]V. Savona, L. Andreani, P. Schwendimann, and A. Quattropani, Solid State Commun. **93**, 733 (1995).
[14]J. Feist and F. J. Garcia-Vidal, Phys. Rev. Lett. **114**, 196402 (2015).
[15]S. Faez, P. Türschmann, H. R. Haakh, S. Götzinger, and V. Sandoghdar, Phys. Rev. Lett. **113**, 213601 (2014).
[16]A. Alù, M. G. Silveirinha, A. Salandrino, and N. Engheta, Phys. Rev. B **75**, 155410 (2007).
[17]R. Fleury and A. Alù, Phys. Rev. B **87**, 201101 (2013).
[18]H. Kelkar, D. Wang, B. Hoffmann, S. Christiansen, S. Götzinger, and V. Sandoghdar, *European Quantum Electronics Conference* (Optical Society of America, 2015), p. EG_6_1.
[19]A. Benz, S. Campione, J. F. Klem, M. B. Sinclair, and I. Brener, Nano Lett. **15**, 1959 (2015).
[20]Z. Lai, N. K. Preketes, S. Mukamel, and J. Wang, J. Phys. Chem. B **117**, 4661 (2013).
[21]D. Abramavicius, D. V. Voronine, and S. Mukamel, Proc. Natl. Acad. Sci. U. S. A. **105**, 8525 (2008).
[22]R. Venkatramani and S. Mukamel, J. Chem. Phys. **117**, 11089 (2002).
[23]A. Piryatinski, V. Chernyak, and S. Mukamel, Chem. Phys. **266**, 311 (2001).
[24]C. Greve, N. K. Preketes, H. Fidder, R. Costard, B. Koeppe, I. A. Heisler, S. Mukamel, F. Temps, E. T. Nibbering, and T. Elsaesser, J. Phys. Chem. A **117**, 594 (2013).
[25]J. A. Cwik, P. Kirton, S. De Liberato, and J. Keeling, preprint arXiv:1506.08974 (2015).
[26]S. Mukamel, *Principles of Nonlinear Optical Spectroscopy* (Oxford University Press, 1999), Vol. 6.
[27]G. Nardin, Semicond. Sci. Technol. **31**, 023001 (2015).
[28]N. Takemura, S. Trebaol, M. Anderson, V. Kohnle, Y. Léger, D. Oberli, M. T. Portella-Oberli, and B. Deveaud, Phys. Rev. B **92**, 125415 (2015).
[29]H. Oka and H. Ishihara, Phys. Rev. B **78**, 195314 (2008).
[30]H. Oka and H. Ishihara, Phys. Rev. Lett. **100**, 170505 (2008).
[31]V. Chernyak, W. M. Zhang, and S. Mukamel, J. Chem. Phys. **109**, 9587 (1998).
[32]D. Abramavicius, B. Palmieri, D. V. Voronine, F. Sanda, and S. Mukamel, Chem. Rev. **109**, 2350 (2009).
[33]O. Roslyak, G. Gumbs, and S. Mukamel, Nano Lett. **10**, 4253 (2010).
[34]See supplementary material at http://dx.doi.org/10.1063/1.4944492 for total Hamiltonian of system in polariton basis and respective singly and doubly excited manifold (Eqs. (S1)-(S8)). Figures S1-S10 show dispersive and absorptive parts of the DQC signals shown in maintext. Figures S11 and S12 shows respective peak splittings.
[35]T. Hayashi and S. Mukamel, J. Mol. Liq. **141**, 149 (2008).
[36]I. V. Rubtsov, J. Wang, and R. M. Hochstrasser, J. Phys. Chem. A **107**, 3384 (2003).
[37]A. Barth, Biochim. Biophys. Acta, Bioenerg. **1767**, 1073 (2007).
[38]L. P. DeFlores, Z. Ganim, S. F. Ackley, H. S. Chung, and A. Tokmakoff, J. Phys. Chem. B **110**, 18973 (2006).
[39]H. Deng, H. Haug, and Y. Yamamoto, Rev. Mod. Phys. **82**, 1489 (2010).
[40]E. R. Bittner, S. Zaster, and C. Silva, Phys. Chem. Chem. Phys. **14**, 3226-3233 (2012).
[41]S. Zaster and E. R. Bittner, Int. J. Mod. Phys. B **29**, 1550157 (2015).
[42]J. Kasprzak, M. Richard, S. Kundermann, A. Baas, P. Jeambrun, J. Keeling, F. Marchetti, M. Szymańska, R. Andre, J. Staehli *et al.*, Nature **443**, 409 (2006).
[43]J. D. Plumhof, T. Stöferle, L. Mai, U. Scherf, and R. F. Mahrt, Nat. Mater. **13**, 247 (2014).
[44]M. Kowalewski, G. Morigi, P. W. Pinkse, and R. de Vivie-Riedle, Phys. Rev. A **84**, 033408 (2011).